Universidade de Lisboa

Instituto Superior técnico

Identification and Computer Control of a Flexible Robot Arm Joint

Part I

Computer Control

Autores:

Ana Catarina Silvestre(81316)

Diogo Oliveira(81844)

Margarida Nabais(81573)

Pedro Soares(81585)

Professor:

João Pedro Gomes

Grupo:

40, 5ª feira, L07

December 13, 2018

1 Introduction

The aim of this work is the identification and computer control design for the position of a flexible joint of a robot arm. The work was divided into two parts. Part I, which is addressed in this report, consists on the utilisation of System Identification methods to obtain a plant model that relates the motor that drives the arm with the angular position of its tip. Part II consists on the design, implementation and testing of a LQG controller for the identified system.

The plant to be controlled is a single joint of a flexible robot arm that is powered by a DC motor, driven by a power amplifier, and the control objective is to actuate the motor so the tip of the bar tracks a specified angle. Fulfilling this control objective is a nontrivial task.

1.1 Nontrivial Control Objective

Let us consider applying a constant input to the system, this means feed the DC motors power amplifier with a constant signal. Applying such a signal is not equivalent to having a constant target tip angle. In this scenario the arm will start spinning at a constant speed for as long as the input signal remains constant. This is a strong indication that the plant has at least one pole as it performs an integration of the input, the input corresponds to the speed of the motor while the variable to be controlled is the position of the arm tip.

However, if the plant were a pure integrator a feedback with a proportional controller would be enough to fulfil the control objective. This is not the case since the robot arm is flexible.

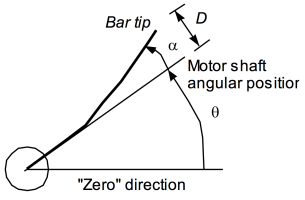

Figure 1: Top view of the plant displaying the distortion of the flexible bar.

The flexibility of the arm conjoined with its inertia causes the tip of the arm to deviate from the motor shaft angular position. This dynamic can be simplified by assuming that the distortion of the arm is caused by a hinge

effect in the middle of a rigid arm and the inertial mass is concentrated on the tip of the arm.

The simplification made can be extended by adding one hinge to all segments of the arm and then dividing the inertial mass among the new segments. This process can be repeated to approximate the plant model. In this approximation every time a hinge is added a new pair of complex conjugate poles is added, being of higher frequency at each iteration.

Additionally, the dominant oscillatory answer with low damping is caused by two complex conjugated poles. It was also observed that there was another oscillatory behaviour in high frequency with a smaller amplitude that can be explained with an additional pair of complex conjugated poles.

There is also a whipping effect since in the beginning the tip of the bar is not able to follow the movement of the motor, which originates a non minimum phase zero, i.e, a zero outside the unit circle.

2 Interface with Computer

The input of the plant in the open-loop conditions described is a voltage signal that after being amplified by the power amplifier controls the DC motor. When a constant non-zero voltage is applied to the system the arm spins at a constant speed as the voltage controls the speed of the motor.

2.1 Sensor Calibration

The interface with the system is made through two sensors, a potentiometer and a strain gauge. This first one measures the shaft angle θ and the second the deformation of the robots arm, which means, the deflection angle of the flexible bar α.

It is known that the total angle of the tip of the flexible bar is given by the sum of two angles

$$y = \theta + \alpha \qquad [degree] \tag{1}$$

So, in order to relate physical variables with electrical tensions, we need to estimate the values of the constants K_p and K_e. In figure 2 is presented the block diagram used to perform the different experiments, being the only difference between those two the motors command signal.

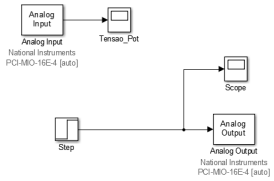

Figure 2: Schematic in SIMULINK used to determine the sensors parameters.

2.2 Calibrate the Potentiometer K_p

The constant K_p that relates the shaft angle with the sensor output is given by

$$\theta = K_p \theta_e \Leftrightarrow K_p = \frac{\theta}{\theta_e} \quad [^\circ \, \mathrm{V}^{-1}] \tag{2}$$

Experimentally, this was obtained by applying a constant signal input, a step signal of $1V$, to the motor and observing the variation of θ_e. As it can be seen in figure 3, θ_e increases linearly while the bar moves away from it's initial position. The discontinuity corresponds to the point where the shaft angle crosses from $-180°$ to $180°$, or vice versa, defined on the potentiometer as the point where the voltage crosses from its maximum to its minimum or vice versa.

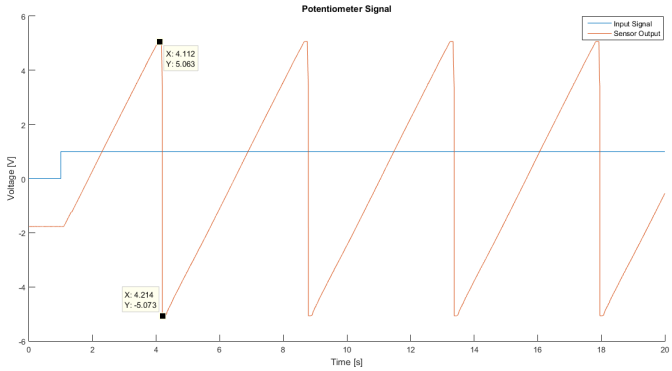

Figure 3: Evolution of the shaft angle applying as an input a constant signal.

Given equation 2 and having the maximum and minimum values obtained from the experiments, we have

$$K_p = \frac{\Delta\theta}{\Delta\theta_e} = \frac{180 - (-180)}{5.0635 - (-5.0732)} = 35.5145 [^\circ \, \mathrm{V}^{-1}] \tag{3}$$

2.3 Calibrate the Strain Gauge K_e

The strain gauge measures the deflection of the bar. To obtain the value of the constant K_e, several deflections of the bar were made using a calibration comb. Using this comb we were able to measure different deflection levels of the bar tip (l) and knowing that $D = 40$cm, we get the values of α through

$$\alpha = arctan(\frac{l}{D}) \tag{4}$$

The results obtained during the experiment to calculate K_e are shown in figure 4.

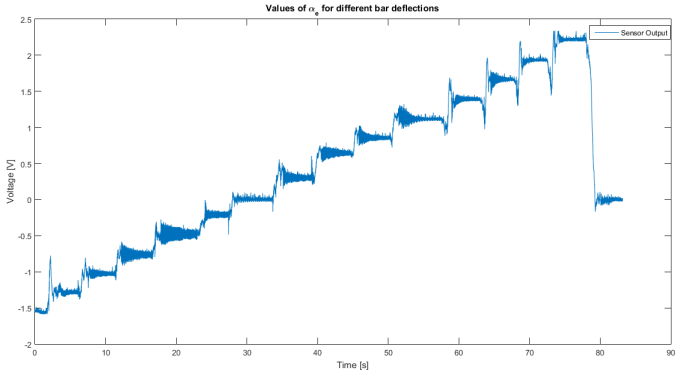

Figure 4: Electrical tension α_e.

The experiment measures are presented in the table 1. Figure 5 represents the dynamics of the flexible bar and shows how to compute α according to D and l using equation 4.

Table 1: Measured values to estimate K_e.

Position	l [cm]	α [°]	α_e [V]
1	-3.7	-1.5535	5.2848
2	-3.05	-1.2863	4.3604
3	-2.4	-1.0245	3.4336
4	-1.8	-0.7624	2.5766
5	-1.1	-0.4796	1.5752
6	-0.5	-0.2094	0.7162
7	0	0.0028	0
8	0.6	0.3024	-0.8594
9	1.4	0.6446	-2.0045
10	2	0.8558	-2.8624
11	2.65	1.1164	-3.7903
12	3.3	1.3888	-4.7162
13	3.9	1.6651	-5.5687
14	4.55	1.9353	-6.4895
15	5.2	2.2152	-7.4069

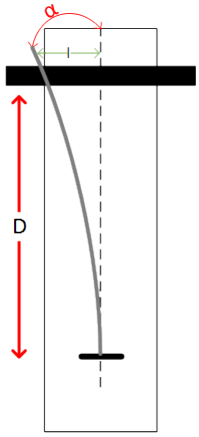

Figure 5: Draw of the flexible bar moving.

To compute α_e for each l, it was gathered data at each l until the ruler more or less stabilised, the output of the sensor was close to stable. Since it was impossible to stabilise the output completely, it was done a mean between the points where the position of the ruler was more or less constant for each l. For each α_e it was used between the 0.5 and 2 seconds of data.

Then, since α and α_e are inversely proportional, a linear regression was made to estimate the relation, K_e, which can be seen in figure 6.

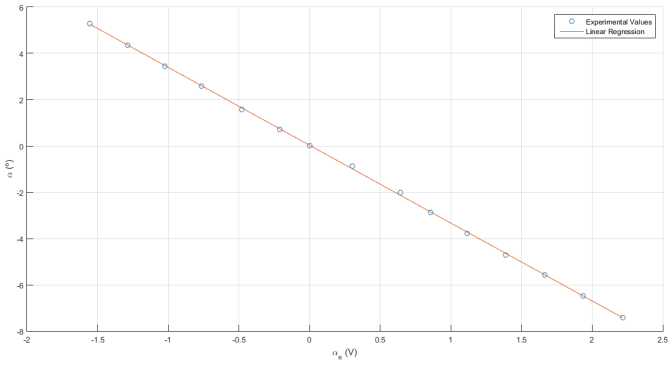

Figure 6: Linear regression to obtain K_e.

The conversion constant K_e is given by

$$\alpha = K_e \alpha_e \Leftrightarrow K_e = \frac{\alpha}{\alpha_e} \quad [^\circ \, \mathrm{V}^{-1}] \tag{5}$$

Using linear regression with the values from table 1 it was obtained a constant value of $K_e = -3.3636$.

It is important to note that linear dependency of electrical tension on deflection, as expressed by the given equation, is only true for relatively small deflections.

2.4 System Characterisation

During the experiments we verified that the motor has a dead zone, which means there is a voltage threshold that has to be reached for the motor to start its movement. As it can be seen in figure 7 this point is at 0.3369V.

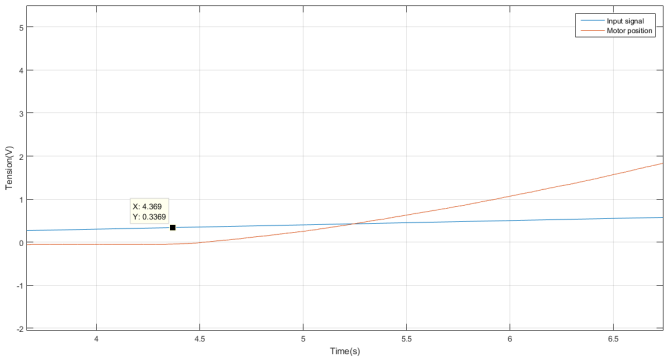

Figure 7: Experiment to determine the dead zone threshold.

3 Plant Model Identification

To identify the plant model, the following steps were performed:

1. Experiments to gather different data;
2. Remove the integral effect by differentiating the motor shaft angle data;
3. Low pass filtering;
4. Detrend the data;
5. Estimate the parameters;

6. Add an integrator;

In 1 the system was excited with both a square and a PRBS waves. In total there were performed 9 measurements, 5 with square waves of $\{0.3, 0.35, 0.4, 0.45, 0.5\}$Hz and 4 PRBS waves with $B = \{0.05, 0.1, 0.15, 0.2\}$.

The models are:

1. PRBS wave with $B = 0.05$;
2. PRBS wave with $B = 0.10$;
3. PRBS wave with $B = 0.15$;
4. PRBS wave with $B = 0.20$;
5. Square wave with $f = 0.40$Hz;
6. Square wave with $f = 0.30$Hz;
7. Square wave with $f = 0.35$Hz;
8. Square wave with $f = 0.45$Hz;
9. Square wave with $f = 0.50$Hz;

Regarding the sampling frequency, as a rule of thumb, it should be chosen such that it is 4 to 10 times faster than the smallest time constant of the plant. We could think that the higher the sampling frequency the better. However, high sampling rates are not ideal as it makes the model have an increased delay, meaning that more variables of the ARMAX would have to be estimated. Consequently, it would require more data to train the ARMAX model and would also increase the estimation. If no more data is provided it will overfit the data since it becomes insufficient. The sampling frequency used was $f_s = 50$Hz.

3.1 Processing the Data

After obtaining the data from the experiments, the data was differentiated. This was done so the integral effect of the system would be removed. The differentiation step is necessary so the following identification methods can be used. This happens because the following steps are performed using the Control Systems Toolbox, that assumes the polynomials are written in the forward shift operator.

The derivation step however increases high frequency noise, figure 8 is an example on how differentiating may increase the high frequency noise.

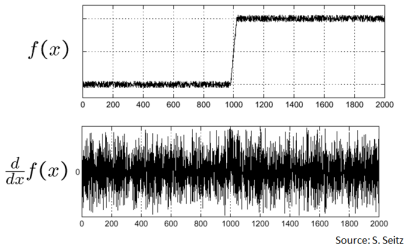

Figure 8: Visual representation of the increase in noise after differentiation.

This increase can be explained by the transfer function of the derivative.

$$X(s) = s \tag{6}$$

Equation 6 shows that the gain of the transfer function increases with the frequency, where the signal to noise ratio is usually lower. The larger gain makes high frequency noise more significant.

So to decrease the influence of the high frequency noise on the obtained model the differentiated signal is filtered with a low pass filter.

Both steps can be achieved using a filter with transfer function of the form

$$H(z) = \frac{(1 - af)z - (1 - af)}{z - af} \tag{7}$$

As shown in figure 9, the bigger the value of af for the filter the smaller the passband of the differentiated signal, which means, the high frequency noise is more attenuated. As af increases, the closer the pole approaches the unit circle, which in terms of the Laplace transform represents the imaginary axis. Increasing af generates slower poles, meaning a lower pole frequency. As a result, they will filter high frequencies.

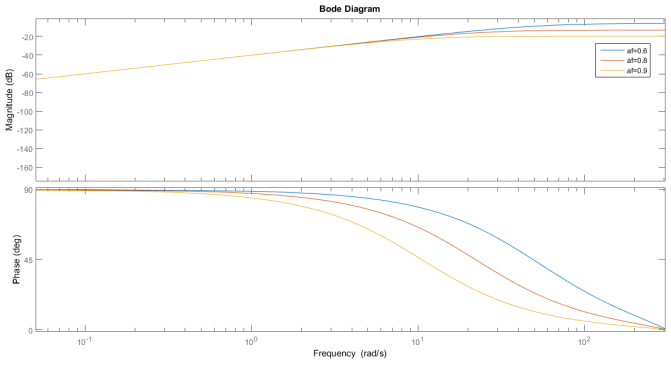

Figure 9: Filter's frequency response.

In figure 9 in the magnitude plot one can identify the differentiation as the segment where the magnitude increases linearly with the frequency. The gain of the filter then stabilises after the cut-off frequency as a result of the low-pass properties of the filter.

Figure 10 shows several time responses with different values of af.

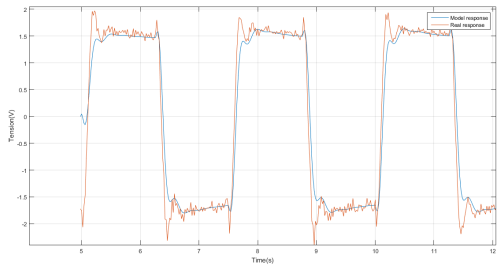

(a) $af = 0.6$

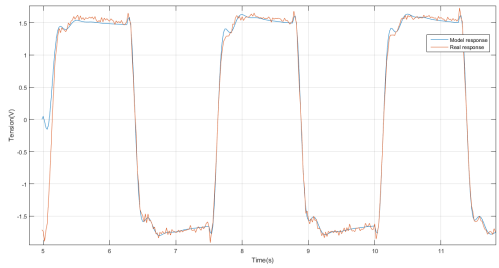

(b) $af = 0.8$

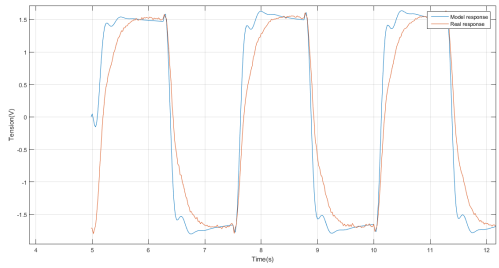

(c) $af = 0.9$

Figure 10: Outputs response with different cutoff frequencies.

From the plots presented in figure 10 one can note that $af = 0.8$ follows the intended signal better than $af = 0.6$ and $af = 0.9$. For $af = 0.9$ the cut-off frequency is too low as the dynamic of the signal is drastically changed. The time constant increased, meaning that the signal shows slower reaction than the real system. As for $af = 0.9$ the cut-off frequency is too high leading

to a lower signal to noise ratio as the increased noise of the high frequency is not adequately filtered.

The differentiation of the systems output also detrends the signal, as such all that remains is to also detrend the input.

With the detrended data the ARMAX model is identified using MATLABs *armax* function, as explained in section 3.2.

After this, an integrator is added, which will undo the differentiation performed to allow the identification of the model. This will add a pole at the origin that had been removed when the differentiation was executed.

3.2 Selecting the Model

After performing the filtering of the data the model is identified using the $ARMAX$ model

$$\begin{aligned} y(k) + a_1 y(k-1) + ... + a_{n_a} y(k-n_a) = \\ b_0 u(k-n_k) + b_1 u(k-n_k-1) + ... + b_{n_b} u(k-n_b) \\ +e(k) + c_1 e(k-1) + ... + c_{n_c} e(k-n_c), \end{aligned} \tag{8}$$

where the parameters that we need to estimate are

- n_a - Auto-regressive part, which defines the number of poles;
- n_b - External part that defines the number of zeros plus 1;
- n_c - Moving Average part;
- n_k - Input-output delay

We only want a pure delay ($n_k = 1$) since it's the minimum delay that we can have that still assures that the system is causal.

To choose the most appropriate model a range of hyperparameters, n_a, n_b, n_c, was chosen to train the $ARMAX$ models. For each combination of hyperparameters and for each dataset a model was trained and the fitness score returned by MATLABs *compare* function used to evaluate the model. From the trained models those that violated causality or that did not had a fit over 89% were discarded. The remaining models are then evaluated throughout all datasets, not just the one that yielded it, and an average is taken.

The selected model was the one with the best fitness score without having a larger than necessary complexity. Less complex models with slightly lower fitness scores were selected instead of better scored complex models, as the latter ones are likely to have overfitted the data.

The results are presented below in table 2.

Table 2: Cross-validation of the models with data sets.

Models/Data Sets	1	2	3	4	5	6	7	8	9	Average
1	91.51	88.28	86.94	87.35	95.79	94.73	95.77	96.10	96.11	92.51
2	83.81	90.00	85.28	83.01	91.98	91.37	91.99	92.95	92.27	89.19
3	88.15	89.59	88.28	86.90	94.75	94.92	95.08	95.97	94.82	92.05
4	91.46	89.58	86.71	89.33	93.88	94.23	94.25	95.29	94.09	94.09
5	83.94	86.01	86.40	83.22	95.75	94.48	95.75	96.24	96.13	90.88
6	84.56	85.93	85.83	83.19	95.14	95.44	95.65	95.54	95.25	90.73
7	83.75	85.18	86.25	82.67	95.45	94.21	95.41	95.95	95.72	90.51
8	83.84	85.77	86.62	82.97	95.40	94.40	95.45	96.19	95.55	90.69
9	83.72	85.63	86.33	82.75	95.41	93.99	95.30	95.71	95.86	90.52

The models that were tested had the following hyperparameters:

1. $n_a = 7, n_b = 3, n_c = 8$;
2. $n_a = 8, n_b = 3, n_c = 8$;
3. $n_a = 7, n_b = 3, n_c = 7$;
4. $n_a = 8, n_b = 3, n_c = 7$;
5. $n_a = 6, n_b = 2, n_c = 7$;
6. $n_a = 4, n_b = 3, n_c = 4$;
7. $n_a = 5, n_b = 2, n_c = 4$;
8. $n_a = 4, n_b = 2, n_c = 4$;
9. $n_a = 5, n_b = 2, n_c = 6$;

3.3 Final Model

The final state-space model will be given by

$$\begin{cases} x(k+1) = Ax(k) + Bu(k) \\ y(k) = Cx(k) + Du(k), \end{cases} \tag{9}$$

where D is a zero matrix and A ,B and C matrices are detailed bellow.

$$A = \begin{bmatrix} 4.33 & -7.64 & 6.87 & -3.16 & 0.59 \\ 1 & 0 & 0 & 0 & 0 \\ 0 & 1 & 0 & 0 & 0 \\ 0 & 0 & 1 & 0 & 0 \\ 0 & 0 & 0 & 1 & 0 \end{bmatrix} \qquad B = \begin{bmatrix} 1 \\ 0 \\ 0 \\ 0 \\ 0 \end{bmatrix} \tag{10}$$

$$C = \begin{bmatrix} -0.05 & 0.14 & -0.09 & 0 & 0 \end{bmatrix}$$

The ARMAX model selected, as stated in section 3.2 had $n_a = 4$,$n_b = 3$, $n_c = 4$. To select the final ARMAX model the characteristics taken into account were the possibility of over or under-fitting.

Some models with high coefficients, like $n_a = 6$,$n_b = 3$, $n_c = 6$, have a higher score value than the model chosen. However, the difference of the fitting values between models can be disregarded as it requires more coefficients, which may over-fit the data. In the other hand, there are models with less coefficients like $n_a = 3$, $n_b = 3$, $n_c = 3$, which also has a higher score value than the model chosen, but this case violates causality as $n_b + n_k$ would be bigger than n_a. There was also a model (8) with $n_a = 4$, $n_b = 2$, $n_c = 4$ that presented a high score value, although lower than the one that we chose. Nevertheless, this particular choice of parameters will also be considered in the next laboratory sessions in order to assure that the proper model is chosen.

The final transfer function is given by

$$G(z) = \frac{Y(z)}{U(z)} = C(zI - A)^{-1}B \tag{11}$$

For the chosen model the final transfer function is

$$G(z) = \frac{-0.05z^4 + 0.14z^3 - 0.09z^2}{z^5 - 3.33z - 4.33z^4 - 7.64z^4 - 6.87z^2 + 3.16z + 0.59z} \tag{12}$$

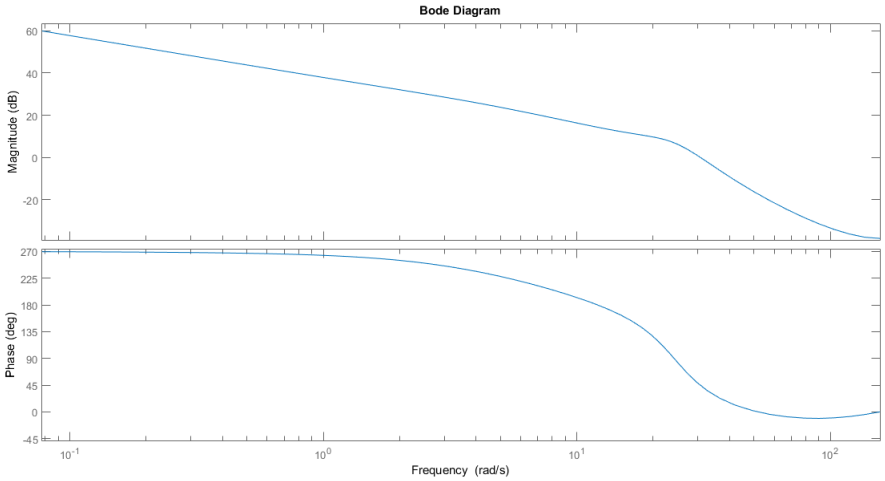

Figure 11: Bode Diagram of the final model..

In figure 11 the frequency response of the system is displayed. As expected higher frequencies have a smaller gain than low frequencies. The deflection of the flexible arm filters higher frequencies as it slows sudden movements due to inertia, favouring its own fundamental frequency. The bode plot also shows a gain inversely proportional to the frequency for low frequencies, this behaviour is explained by the integrator. Since the position of the tip of the flexible arm is the variable to be controlled the relation to the motors input voltage is an integrator which is represented in frequency as an inverse proportionality to the frequency.

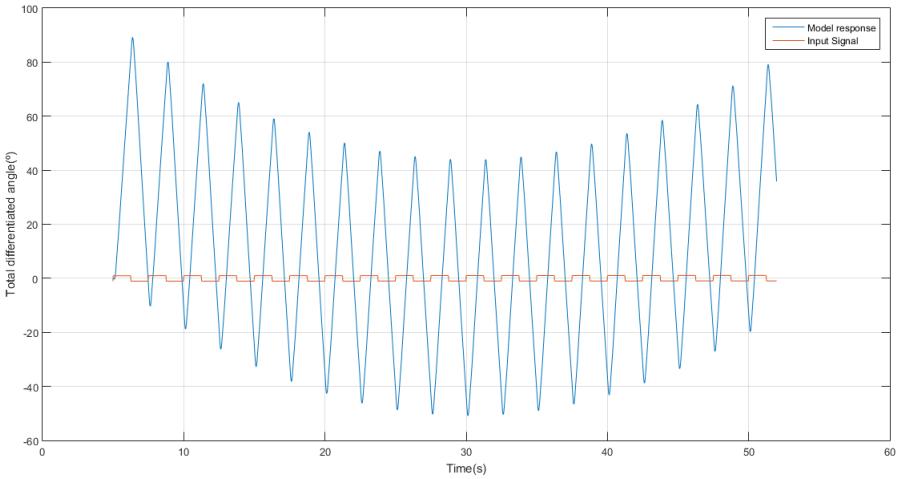

Figure 12: Time response of the identified model.

Figure 12 shows the estimated models response to a square wave. The triangular response to the square wave is the expected result due to the integrator effect of the system. The concavity of the response is similar to the variations observed on the real system and may be due to the effects of the flexible bar on the systems dynamic.

The zero-pole representation of the model is shown bellow in figure 13.

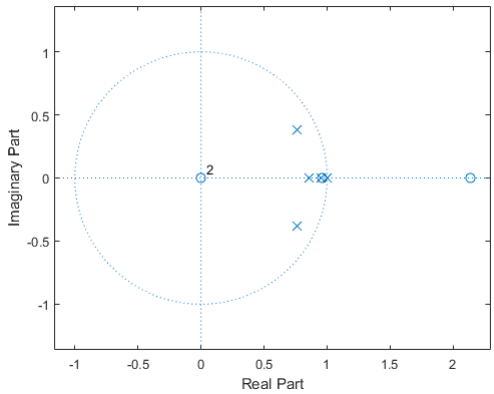

Figure 13: Model pole-zero plot.

It can be observed that there are 5 poles and 4 zeros. The conjugated complex poles correspond to the fundamental frequency of the bar. The pole in $z = 1$ represents the integral effect of controlling the position of

the tip rather than its angular velocity. The two remaining poles in the z axis correspond to the motor dynamic that relates the input voltage to the angular velocity. It is important to note the zero outside the unit circle, is a non-minimum phase zero, which describes the whiplash effect observed.

3.4 Changing the Sampling Frequency

We have also tested what would happen if we doubled our original sampling frequency in order to verify if the model would be prepared to simulate those conditions.

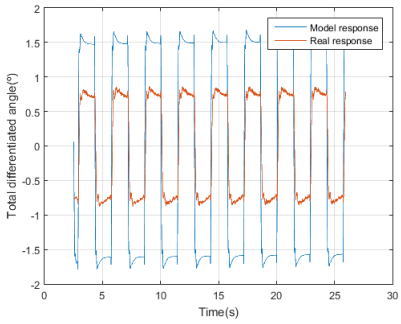

Figure 14: Model response for with a sapling frequency $100Hz$

As expected, the model was not able to simulate correctly the real effect being notable that the model thinks the effect of the input is much bigger than the reality because is trained for the system to be under the effect of the same signal for longer.

4 Conclusion

After the experiment's analysis we can conclude that all the goals were achieved for this first part as we successfully determined the calibration parameters and identified the system's model based on the gathered data.

In terms of the calibration parameters of the sensors, we obtained similar results to those that were indicated by the professor. We could have improved them by making more measurements in order to decrease the variance of the estimations to the real model.

Regarding the systems identification, after performing several experiments with different wave forms we estimated several models, evaluated each one

and chose the most appropriate model's coefficients. As a result we ended up with a 5^{th} order polynomial with 5 poles and 4 zeros with a pure delay.